Front. Environ. Sci. Eng. 2024, 18(1): 2
https://doi.org/10.1007/s11783-024-1762-0

RESEARCH ARTICLE

Synergistic promotion of particulate matter reduction and production performance via adjusting electrochemical reactions in the zinc electrolysis industry

Zizhen Ma[1,2], Jingkun Jiang[2], Lei Duan[2], Jianguo Deng[2], Fuyuan Xu (✉)[3], Zehui Li[4], Linhua Jiang (✉)[3], Ning Duan (✉)[3]

1 School of Environmental and Municipal Engineering, Qingdao University of Technology, Qingdao 266520, China
2 State Key Joint Laboratory of Environmental Simulation and Pollution Control, School of the Environment, Tsinghua University, Beijing 100084, China
3 State Key Laboratory of Pollution Control and Resources Reuse, College of Environmental Science and Engineering, Tongji University, Shanghai 200092, China
4 School of Physics, Peking University, Beijing 100871, China

HIGHLIGHTS

- Electrolytic PM can be reduced by controlling operation parameters.
- The optimization conditions exist, reducing PM without deteriorating PC and CE_{Zn}.
- Abatement essence is to inhibit gas evolution reactions.

GRAPHIC ABSTRACT

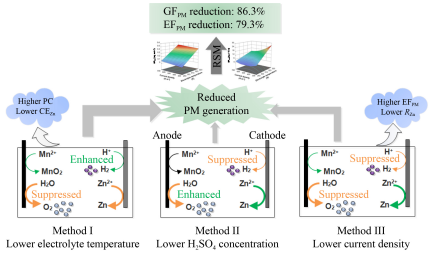

ARTICLE INFO

Article history:
Received 27 February 2023
Revised 3 July 2023
Accepted 4 July 2023
Available online 10 August 2023

Keywords:
Zinc electrolysis
Particulate matter
Energy consumption
Operating parameters
Bubble characteristic
Electrochemical reaction

ABSTRACT

Heavy particulate matter (PM) pollution and high energy consumption are the bottlenecks of hydrometallurgy, especially in the electrolysis process. Therefore, an urgent need is to explore PM reduction methods with production performance co-benefits. This study presents three PM reduction methods based on controlling operating parameters, i.e., lowering electrolyte temperature, H_2SO_4 concentration, and current density of the cathode. The optimized conditions were also investigated using the response surface methodology to balance the PM reduction effect and Zn production. The results showed that lowering electrolyte temperature is the most efficient, with an 89.0% reduction in the PM generation flux (GF_{PM}). Reducing H_2SO_4 concentration led to the minimum side effects on the current efficiency of Zn deposition (CE_{Zn}) or power consumption (PC). With the premise of non-deteriorating CE_{Zn} and PC, GF_{PM} can be reduced by 86.3% at the optimal condition (electrolyte temperature = 295 K, H_2SO_4 = 110 g/L, current density = 373 A/m^2). In addition, the reduction mechanism was elucidated by comprehensively analyzing bubble characteristics, electrochemical reactions, and surface tension. Results showed that lower electrolyte temperature inhibited the oxygen evolution reaction (OER) and compressed gas volume. Lower H_2SO_4 concentration inhibited the hydrogen evolution reaction (HER) and reduced electrolyte surface tension. Lower current density inhibited both OER and HER by decreasing the reaction current. The inhibited gas evolutions reduced the microbubbles' number and size, thereby reducing GF_{PM}. These results may provide energy-efficient PM reduction methods and theoretical hints of exploring cleaner PM reduction approaches for industrial electrolysis.

✉ Corresponding authors
E-mails: fuyuanxu@tongji.edu.cn (F. Xu); jianglinhuann@163.com (L. Jiang); ningduan2020@163.com (N. Duan)

1 Introduction

Particulate matter (PM) is inevitable during industrial

electrolysis (Ma et al., 2020b; Xu et al., 2020b). Generated PM is highly acidic due to containing acids such as sulfuric acid from zinc electrolysis (Sorour et al., 2017) or chromic acid from chrome electroplating (Shaw et al., 2020). It can also enrich heavy metals with concentrations up to thousands of times greater than in the electrolyte (Ma et al., 2020a). Such PM constitutes carcinogenic and non-carcinogenic occupational hazards to worker health (Ma et al., 2020a; Mokarram et al., 2020) and increases PM concentrations in the atmosphere. There is, therefore, an urgent need to control and reduce PM during industrial electrolysis, especially from the perspective of occupational workers' health.

According to PM generation mechanisms, a fundamental approach to mitigating PM generation at its source involves modulating the characteristics of bubbles and altering the properties of the electrolyte. The PM is generated from the bubbles bursting at the liquid interface, including jet and film droplets (Wang et al., 2017; Deike et al., 2022). There are quantitative relationships between the bubble characteristics and the PM generation. For example, no film droplets form when the diameter of a bubble in seawater is < 1.00 mm (Wang et al., 2017), and no jet droplets form when the bubble diameter in pure water is < 8.00 μm (Ji et al., 2011). Properties of the solution, especially surface tension, also affect the total mass of PM formed, possibly by changing the thickness of the bubbles film (Ke et al., 2017). Specific to the electrolysis process, it is verified that bubble size has a noticeable effect on the amount of acid mist (Berny et al., 2021; Deike et al., 2022). The bubbles critical to PM formation are from electrochemical gas evolution reactions (usually oxygen evolution reaction (OER) and the hydrogen evolution reaction (HER) (Luo et al., 2018; He et al., 2021). However, how the electrochemical reactions affect the formation of PM remains to be further explored.

Some effective methods for PM reduction have been put forward based on the preceding mechanisms and relationships. These include employing surfactants to reduce acid mist (Xu et al., 2020b), using ultrasonication (Ma et al., 2020b), and adopting a floating porous phase (Qu et al., 2022), and adjusting operating parameters (Al Shakarji et al., 2011b). Energy consumption and production productivity pose significant challenges to the integration of these methods into industrial practices, particularly in the context of the ongoing energy crisis and climate change (Xu et al., 2020a; Dwivedi et al., 2022). For instance, organic surfactants designed for acid mist prove to be highly efficient, modifying electrolyte surface tension or viscosity (Al Shakarji et al., 2013). However, they can present a host of issues: they may be chemically and thermally unstable, costly, toxic, or flammable. Moreover, they may augment energy consumption by a range of 3.43%–10.3% (Dhak et al., 2011; Sorour et al., 2017). Ultrasonication can reduce the size and number of bubbles (Bouakaz et al., 2005; Theerthagiri et al., 2020). It has been used to reduce PM generation during zinc electrolysis (Ma et al., 2020b) and chromium electroplating (Mason et al., 2001). Ultrasonication requires massive ultrasonic energy consumption despite saving 2.25% electrolysis energy consumption (Ma et al., 2020b). This barrier makes ultrasonication unusable in industrial applications in the foreseeable future. Electrode caps that allow bubbles to coalesce into more giant bubbles were invented and fixed to anodes to reduce PM emission by > 90% (Papachgristodoulou et al., 1985; Dusen and Smith, 1989). However, they did not affect PM < 1.00 μm in diameter, and none has been adopted for use in industrial operations (Mcginnity and Nicol, 2014). It is noteworthy that during copper electrolysis, alterations in operating parameters, including electrolyte temperature, current density, and H_2SO_4 concentration, can affect the generation of acid mist by modifying the nature of the electrolyte (Al Shakarji et al., 2013). This result indicates that adjusting operating parameters may be a practical way of PM for industrial electrolysis. However, the particular efficacies of altering these operating parameters on PM reduction and production performance are still unclear. Moreover, the specific reduction mechanisms involving electrochemical reactions, bubble characteristics, and surface tension remain to be investigated comprehensively.

In this study, a laboratory-scaled zinc electrolysis system was designed as a case study to investigate PM reduction efficacies and production performance by adjusting three operating parameters (electrolyte temperature, H_2SO_4 concentration, and current density). The optimal method to balance PM reduction with power consumption (PC) and productivity was also discussed using the response surface method. In addition, the mechanisms driving different ways of PM reduction were identified by analyzing bubble characteristics, electrochemical reactions, and surface tension. The results may provide a theoretical and practical roadmap for incorporating PM reduction in industrial production and indicate optional directions to exploring more effective and practical PM reduction methods for the electrolysis industry.

2 Materials and methods

2.1 Electrolysis experiment

Referring to our previous study (Ma et al., 2020b), galvanostatic zinc electrolysis was performed in a bench-scale home-made polymethyl methacrylate electrolysis cell (200 mm × 105 mm × 160 mm). To avoid the influence of anode age, all anodes were passivated with H_2SO_4 for 24 h and aged with electrolysis for 24 h. The schematic overview and operation details of the electrolysis

experiment are presented in the supporting information (Fig. S1(a)). The electrolyte was prepared with analytical grade H_2SO_4 (> 98.0%), $ZnSO_4{\cdot}7H_2O$, and $MnSO_4{\cdot}H_2O$, which were purchased from the Sinopharm Chemical Reagent Co., China. The concentration of Zn^{2+} was 45.0 g/L, and that of Mn^{2+} was 3.00 g/L based on the industrial electrolyte composition. Electrolysis was performed for four hours and repeated twice for each set of parameters.

2.2 PM sampling and analysis

The flux of generated PM (GF_{PM}) and emission factor of generated PM (EF_{PM}) were measured with Eqs. (1) and (2) using the gravimetric method. GF_{PM} is only related to the PM generation rate, which directly influences the PM concentration in facilities and worker health. In contrast, EF_{PM} is related to both the PM generation rate and Zn deposition rate with relationships to a current density of the cathode, reflecting the PM emission level and the influence on the atmospheric environment. Detailed information on the sampling and analysis methods has been previously published (Ma et al., 2020b). In short, sampling was carried out in a polymethyl methacrylate box (0.5 m × 0.5 m × 1.5 m) with a gas distributor close to the bottom (Fig. S1(b)) to avoid the influence of ambient air. PM generated during electrolysis was collected on a Teflon filter (R2PL047, Pall Co. Ltd., USA) with a sampling flow rate of 16.7 L/min. Six filter samples collected in parallel were used in each test to ensure reliable data for analysis.

$$GF_{PM} = \frac{M_{sample} - M_{blank}}{t} \tag{1}$$

$$EF_{PM} = \frac{GF_{PM}}{R_{Zn}} \tag{2}$$

where M_{sample} is the mass of aerosol or sulfuric acid mist on the filter during electrolysis (g); M_{blank} is the mass of aerosol or sulfuric acid mist on a blank filter (g); t is the sampling time (h); and S is the aerosol generation area of the electrolysis cell (m^2).

2.3 Assessment of production performance

The production performance indicators' values affected by the operating parameters were calculated and analyzed. Impurity content (IC), including Pb, Fe, Cd, Al, Cu, and Sn, affects the quality of the grade of zinc products. $Zn_{99.995}$ is the highest grade of Zn (pure Zn metal) with IC < 0.005%. Detailed classification of zinc grade is given in Table S1. After digestion, the percentages of impurities in the Zn product were analyzed using inductively coupled plasma mass spectrometry (ICP-MS, X series, Thermo Fisher Scientific Co. Ltd., USA). The current efficiency of Zn deposition (CE_{Zn}) is the ratio of theoretical deposited Zn to actual deposited Zn. CE_{Zn} was calculated using Eq. (3) after the Zn deposited on the cathode during electrolysis was weighed. R_{Zn}, the actual rate of Zn deposition, was calculated with Eq. (4). CE_{Zn} and R_{Zn} are two measures of productivity. PC, defined as the energy required for electrolysis to produce a unit mass of Zn (kWh/t Zn), serves as an indicator of the energy consumption associated with electrolysis cost. The cell voltage was measured using a multimeter (the voltage drop between the adjacent cathode and anode plates, V_{cell}). PC was then calculated using Eq. (5).

$$CE_{Zn} = \frac{M_{Zn}}{1.22 \times I \times t} \times 100\%, \tag{3}$$

$$R_{Zn} = \frac{M_{Zn}}{t}, \tag{4}$$

$$PC = \frac{V_{cell}}{q \times CE_{Zn}} \times 1000. \tag{5}$$

where M_{Zn} is the mass of Zn deposited on the cathode (g); I is the current (A); t is the time duration of electrolysis (h); V_{cell} is the cell voltage (V); and q is the electrochemical equivalent, referring to the amount of electrolytic metal produced by 1 Coulomb (C) of electricity, 1.22 g/A/h for Zn.

2.4 Characterization and analysis

2.4.1 Measurement of bubble characteristics

Bubble characteristics under different operating conditions were observed and analyzed according to a previously published method (Ma et al., 2020b). A continuous wave laser (7 W) with a 1 mm width beam illuminated the area under observation (22 mm × 40 mm × 1 mm). A 16-bit CMOS high-speed camera (PCO. Edge, PCO Co., Ltd., Germany) with a Canon EF 100 mm f/2.8 macro USM lens was used to capture bubble images. The bubbles were filmed at 50 Hz with an exposure time of 200 μs at a resolution of 2560 × 2160 pixels. The images were segmented by PIV-view software using thresholding, and the number and size of the bubbles were automatically counted by phase-size estimation software. Image resolution allowed bubbles ⩾ 20 μm diameter to be observed. This method semiquantitatively indicates the number and size of the bubbles, although the concentration of bubbles varies at different locations in the system.

2.4.2 Quantification of gas production

The current efficiencies of OER (CE_{OER}) and HER (CE_{HER}) and the gas generation rates (R_i) were estimated to quantify the amount of gas produced. Electrolyte at the inlet and outlet of the electrolysis cell was collected to quantify dissolved Mn; the current efficiency of Mn^{2+}

oxidation (CE_{Mn}) was then calculated using Eq. (6). Next, CE_{OER} was calculated using Eq. (7), which ignored the effect on the current efficiency of Pb corrosion (Zhang et al., 2018), and CE_{HER} was calculated using Eq. (8). Finally, the gas generation rates of O_2 (R_{O_2}) and H_2 (R_{H_2}) were also calculated by Eq. (9):

$$CE_{Mn} = \frac{(C_{in} - C_{out}) \times V \times n \times F}{I \times t} \times 100\%, \quad (6)$$

$$CE_{OER} = 100\% - CE_{Mn}, \quad (7)$$

$$CE_{HER} = 100\% - CE_{Zn}, \quad (8)$$

$$R_i = \frac{I \times CE_i \times V}{n \times F}, \quad (9)$$

where C_{in} and C_{out} represent the respective concentrations of Mn dissolved in the electrolyte at the cell inlet and outlet (mol/L); V is the volume of the electrolyte (L); n is the number of electrons participating in the reaction. In this case, $n = 2$ due to the reaction product being the solid MnO_2. F is the Faraday constant (C).

2.4.3 Electrochemical characterization

Linear sweep voltammetry (LSV) was used to explain the changes in electrochemical reactions and energy consumption under different operating parameters. Using a three-electrode system, the experiments were conducted on an electrochemical workstation (CHI608D, Shanghai CH Instruments Company in China). A saturated mercury sulfate electrode (MSE) was selected as the reference electrode to avoid introducing additional impurities. For anodic reactions, a lead-based alloy with an effective area of 1 cm^2 was used as the working electrode, and an aluminum sheet with an area of 6 cm^2 was used as the counter electrode. The starting and ending voltages of linear scanning were 1.26 and 1.60 V. Pure aluminum with a geometric area of 0.79 cm^2 was used as a working electrode, and a graphite plate of 6.00 cm^2 was used as the counter electrode for cathodic reactions. The starting and ending voltages of linear scanning were −1.46 and −1.85 V, respectively. The scan rates for anodic and cathodic reactions were 0.001 V/ms. Before the experiment, the working electrode was sanded with 1200-grade sandpaper until its surface was smooth, and the electrode surface was washed with absolute ethanol, followed by high-purity water.

2.4.4 Measurement of surface tension of the electrolyte

Surface tension was also measured to identify its effects on PM generation under variable operating parameters. An automatic surface tension meter (K100, KRUSS, Germany) using a Wilhelmy plate was used to measure the surface tension of the electrolyte for various temperatures and different H_2SO_4 concentrations.

2.5 Experiment design and optimization parameters

A single-factor laboratory experiment was designed to identify the specific influence of electrolyte temperature, the current density of the cathode, and H_2SO_4 concentration on PM generation. Table S2 shows the values set for each parameter. The values of these three parameters were chosen based on industrial zinc electrolysis practices. The response surface methodology (RSM) based on central composite design (CCD) optimized the PM reduction rate and zinc production performance. The experiment matrix was designed by Design-Expert® Software Version 12, and the design scheme consisted of 15 experimental runs with each variable evaluated at three levels (Table S3). Statistical significance and adequacy of the model were examined by ANOVA and determined by Fisher's F-test, respectively. The effects of independent parameters on GF_{PM}, EF_{PM}, CE_{Zn}, and PC were fitted using multivariate regression analysis. The polynomial expressions and the probability values (p-value) of Fisher's F-test were also analyzed.

3 Results and discussion

3.1 PM reduction by optimizing the operating parameters

As Figs. 1(a) and 1(b) shows, GF_{PM} was positively correlated with electrolyte temperature, H_2SO_4 concentration, and current density. EF_{PM} varied in the same way as GF_{PM} with the change of electrolyte temperature and H_2SO_4 concentration but decreased first and then increased as current density increased. For example, as the electrolyte temperature increased from 298 to 328 K, GF_{PM} rose from 14.6 to 258 g/h, and EF_{PM} increased from 1.27 to 22.5 kg/t Zn. Unlike GF_{PM}, the minimum value of EF_{PM} (9.83 kg/t Zn) appeared at 500 A/m^2 when the current density increased because it is affected by both GF_{PM} and the Zn deposition rate. The analysis of variance for the single factor showed that the difference among the three treatments is statistically significant ($p < 0.0001$). These results indicate that PM generation reduction can be accomplished in three ways: decreasing electrolyte temperature, reducing H_2SO_4 concentration, or decreasing current density. Of the three methods identified, lowering the electrolyte temperature is the most effective, second only to using the most efficient surfactants, and diminishing the H_2SO_4 concentration is the least effective. Specifically, starting with conventional values of the three operating parameters (313 K, 160 g/L, 500 A/m^2), GF_{PM} was reduced by 89.0%, 12.6%, and 19.1% if the parameters decreased to 298 K, 110 g/L, and 300 A/m^2. The GF_{PM} at different electrolyte temperatures and current densities are the same as those obtained in a previous study of copper electrolysis (Al Shakarji et al., 2013). Contrary to this study which suggests that higher

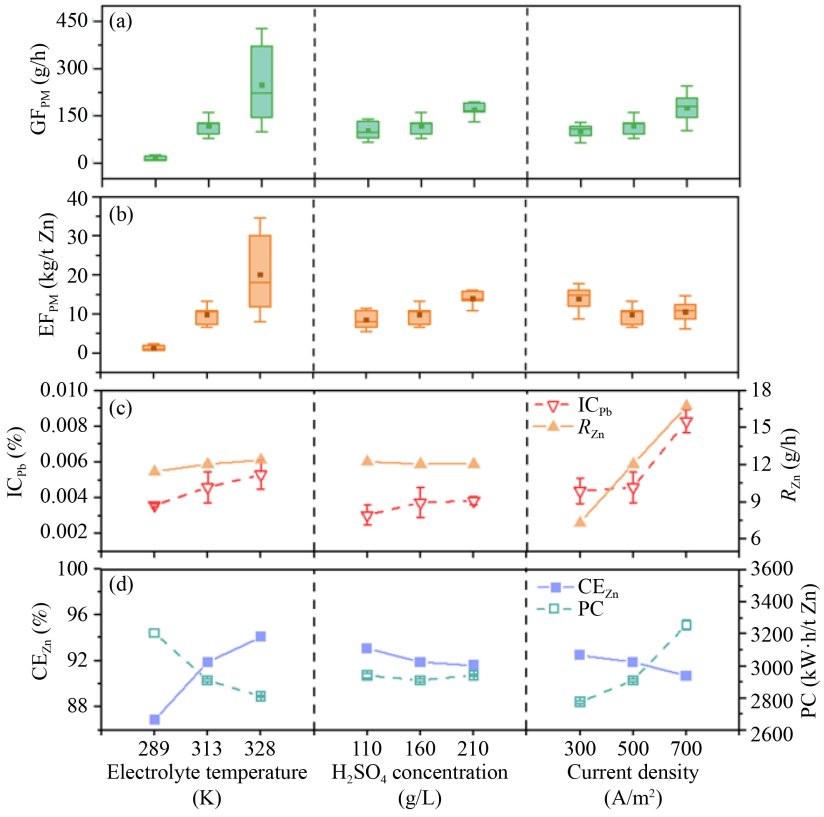

Fig. 1 Influences of three operational parameters on (a) the generation flux of aerosols (GF_{PM}), (b) emission factor of PM (EF_{PM}), (c) Pb content in the Zn product (IC_{Pb}) and Zn deposition rate (R_{Zn}), and (d) current efficiency of Zn deposition (CE_{Zn}) and PC.

acidity results in lower acid mist, our proposed adjustment of H_2SO_4 concentration presents a contrasting viewpoint. The difference may be explained by copper electrolysis having different electrolytes and using other electrode materials, so the H_2SO_4 concentration affects the gas evolution reactions differently.

In addition to environmental benefits, PC and consequent economic benefits are also concerns that drive practical application. Efficient industrial electrolysis demands higher product output, fewer product impurities, and less energy consumption. The performances of R_{Zn}, CE_{Zn}, IC_{Pb}, and PC were investigated, and their results are shown in Figs. 1(c) and 1(d). Among all impurities, Pb content (IC_{Pb}) was only discussed here due to the negligible percentages of other impurities, such as Cd and Fe (Table S4). It is favorable that the three methods of reducing PM generation all improved product quality with Pb reduction by 4.35%–21.7% (Fig. 1(c)) compared with conventional electrolysis. The other three performance indicators became significant factors in the industrial application of these three methods. With the increasing electrolyte temperature, R_{Zn} and CE_{Zn} increased obviously, but PC decreased. When H_2SO_4 concentration increased from 110 to 210 g/L, R_{Zn}, CE_{Zn}, and average PC, all decreased slightly. As current density increased, R_{Zn} and PC increased, but CE_{Zn} decreased. These results indicate the drawbacks of the three PM reduction methods. Specifically, reducing the electrolyte temperature resulted in lower CE_{Zn} and an additional 10.7% power. A reduction in H_2SO_4 concentration bolstered Zn productivity, though the PM reduction efficiency remained minimal and was associated with a slight increase in PC. A decrease in current density, on the other hand, led to a reduced R_{Zn} and a higher EF_{PM}. Overall, a contradiction appears to exist between the PM reduction rate and certain production performance indicators.

To balance the PM reduction rate with performance indicators, the results from the CCD design based on RSM methodology were analyzed to find the optimal operational parameter combination. Polynomial expressions and the probability values (p-value) of Fisher's F-test are demonstrated in SI (S.1). The three-dimensional graph of the factors' effects and their combined effects on GF_{PM}, EF_{PM}, CE_{Zn}, and PC are presented in Figs. 2(a)–2(d). For GF_{PM} and EF_{PM}, the influence of the electrolyte temperature and current density proved significant, while the effect of H_2SO_4 concentration was insignificant and ignorable, aligning with the impact of a single factor. GF_{PM} showed a linear response to changes in electrolyte temperature and current density with an adjusted R^2 of 0.893 (Table S5). Meanwhile, EF_{PM} exhibited a quadratic

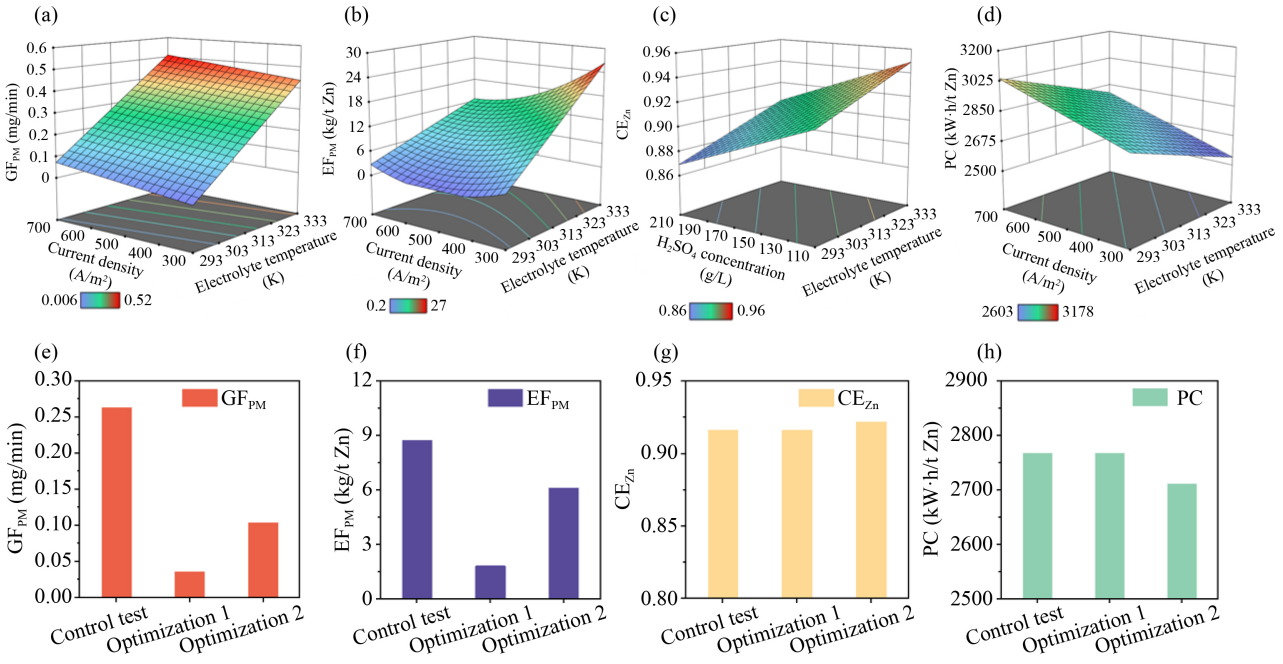

Fig. 2 Response surface graphs showing the effects of operating parameters: (a) generation flux of PM, GF_{PM}; (b) emission factor of PM, EF_{PM}; (c) current efficiency of Zn deposition, CE_{Zn}; and (d) energy consumption by electrolysis, PC. And PM reduction effects and Zn production performance indicators: (e) GF_{PM}; (f) EF_{PM}; (g) CE_{Zn}; and (h) PC, at the optimized conditions. (a, b, and d were drawn at H_2SO_4 concentration of 160 g/L and c was drawn at current density of 500 A/m^2; Optimization 1: 295 K, 110 g/L, and 373 A/m^2; Optimization 2: 301 K, 110 g/L, and 347 A/m^2).

response to electrolyte temperature and current density with an adjusted R^2 of 0.926. The validity of the fitted equations was subsequently corroborated under random conditions.

The obtained polynomial expressions were employed to propose specific operating parameters and further optimize the PM reduction rate and Zn production performance based on multi-objectives. An optimized condition for PM reduction was proposed to be 295 K, 110 g/L, and 373 A/m^2 with the premise of invariable CE_{Zn} and PC. The predicted reduction rates of GF_{PM} and EF_{PM}, illustrated in Figs. 2(e) and 2(f), are 86.3% and 79.3%, respectively. However, unlike PM, the potential for improving CE_{Zn} and PC was slight, with the maximum calculated efficiencies in this study falling below 5.19% and 5.94%, respectively. With the objectives of minimizing GF_{PM} and EF_{PM} and maximizing CE_{Zn} and PC, the parameters were predicted to be 301 K, 110 g/L, and 347 A/m^2.

The corresponding reduction rates of GF_{PM}, EF_{PM}, and PC were 60.4%, 30.2%, and 2.02%, respectively, with an increase of 0.66% in CE_{Zn} (Figs. 2(g) and 2(h)). Despite certain practical constraints—such as the amplification effect during industrial production—these optimized conditions suggest the existence of at least one optimal combination of conditions capable of simultaneously reducing PM generation and emissions, promoting Zn production, and exerting a minimal effect on energy consumption.

3.2 PM reduction mechanisms of varying operating parameters

This section delves into the impacts of adjusting operating parameters on both the reduction of PM generation and the enhancement of Zn production performance from the perspectives of bubble characteristics, surface tension, and electrochemical reactions. An overarching mechanism is outlined to guide further exploration of cleaner reduction methods.

3.2.1 Electrolyte temperature

Electrolyte temperature mainly affects GF_{PM} by changing microbubble characteristics rather than changing surface tension. As Fig. S2(a) shows, surface tension increased as electrolyte temperature decreased. Larger surface tension should increase GF_{PM} because the bubble film is thicker when a bubble bursts at the solute surface (Ke et al., 2017). It has been empirically verified that the electrolyte's surface tension is proportional to the sulfuric acid mist concentration during copper electrolysis (Al Shakarji et al., 2011b). However, in contrast to surface tension, bubble characteristics oppose PM generation at varying electrolyte temperatures. Figs. 3(a)–3(c) shows the number-size distribution of bubbles in electrolyte at different electrolyte temperatures, H_2SO_4 concentrations, and current densities. As the electrolyte temperature decreased, both the number and size of microbubbles

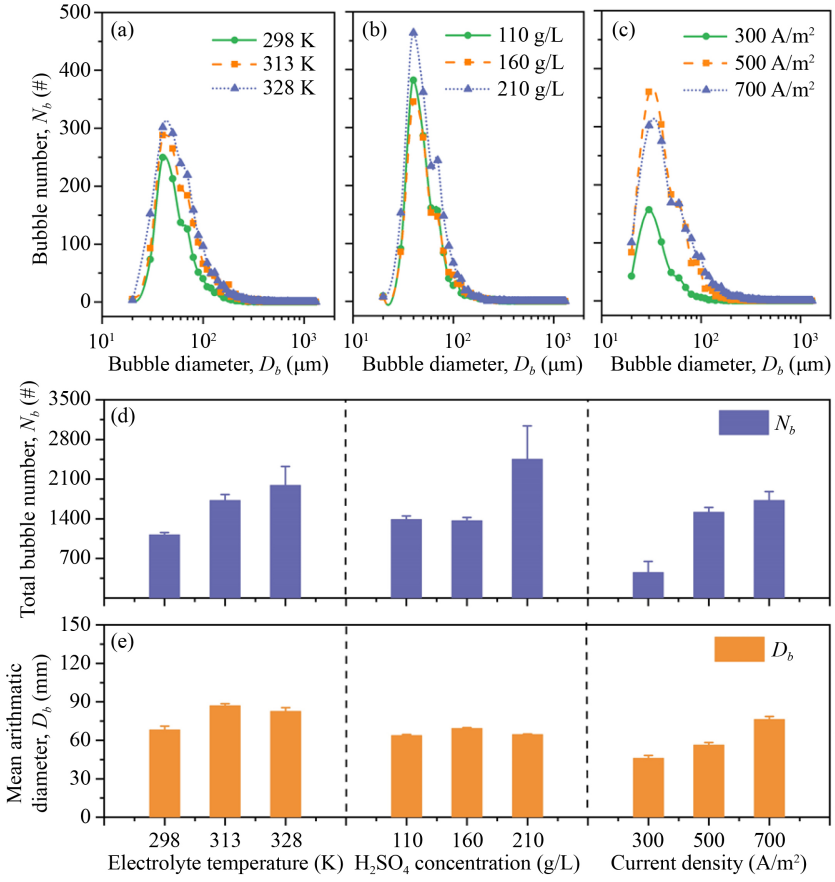

Fig. 3 Bubble characteristics for different operational parameters: (a–c) number–size distribution of bubbles; (d) the total number of bubbles in observed ozone; (e) mean calculated bubble diameter.

diminished, illustrated in Figs. 3(a), 3(d), and 3(e), aligning with the results observed in copper electrolysis (Al Shakarji et al., 2011a). Fewer and smaller microbubbles should contribute to a decline in GF_{PM} (Ma et al., 2020a). The positive correlation between GF_{PM} and electrolyte temperature (Fig. 1(a)) indicates that bubble characteristics are the determinant factors of GF_{PM}. In other words, the reduction in PM generation brought about by the decreased number and size of microbubbles surpassed the increase in PM generation resulting from enhanced surface tension.

The decrease in the number and size of microbubbles at the lower electrolyte temperature may be due to inhibited OER. The current efficiencies of the main electrolytic reactions and the gas evolution rates were calculated with results shown in Figs. 4(a)–4(c). The CE_{OER} at the anode rose from 87.9% to 98.7%, and R_{O_2} increased from 216 to 247 mL/min as the electrolyte temperature increased from 298 to 328 K, demonstrated in Figs. 4(a) and 4(d). The lower CE_{OER} and R_{O_2} at lower electrolyte temperature verified the inhibited OER and less generated O_2. On the cathode, electrolyte temperature variation should affect both Zn deposition and HER. In comparison, Zn deposition should be more susceptible to electrolyte temperature than HER, because the electrolyte temperature influences Zn^{2+} transfer rate more significantly but H^+ concentration in electrolyte is large enough so as to the same surface and bulk concentrations of H^+ (Lasia, 2019). Higher temperature could boost the Zn^{2+} transfer rate, leading to a higher CE_{Zn} (Fig. 1(d)). Thus, the calculated CE_{HER} decreased from 13.1% to 5.95% as the electrolyte temperature increased from 298 to 328 K, presented in Eq. (8). Consequently, the H_2 generation was anticipated to increase, leading to a higher calculated R_{H_2} at a lower electrolyte temperature. It is essential that the decrease in R_{O_2} (38.2 mL/h) was more significant than the increase in R_{H_2} (22.1 mL/h). Therefore, the total gas evolution rate decreased at the lower electrolyte temperature, thus decreasing both the number and size of microbubbles. The lower temperature can also reduce the total gas volume and the size of microbubbles by the ideal gas law under constant mass and pressure conditions (Xue et al., 2019).

The impact mechanism of electrolyte temperature on Zn production performance indicators was also investigated. Variations in polarization curves and dynamic potentials at both anode and cathode are shown in Fig. 5. At the anode, the potentials at a given current

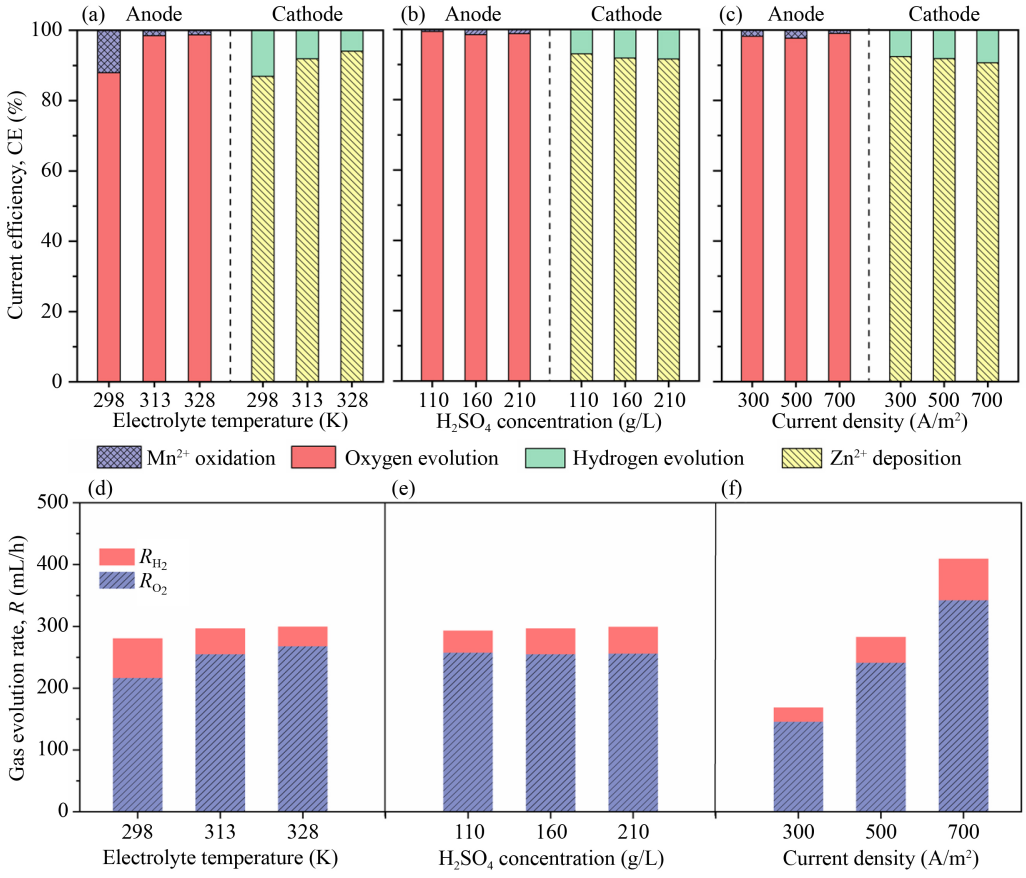

Fig. 4 Current efficiency of electrochemical reactions on anode and cathode for different operational parameters: (a) electrolyte temperature; (b) H_2SO_4 concentration; (c) current density; and gas evolution rates for three operational parameters: (d) electrolyte temperature; (e) H_2SO_4 concentration; (f) current density.

density of 50 mA/cm^2 were 1.482, 1.417, and 1.407 V at electrolyte temperatures of 298, 313, and 328 K with Mn^{2+} (Fig. 5(a)). The anodic polarization curve, depicted in the absence of Mn^{2+} in the electrolyte, representing soly OER activity at the anode, exhibits a similar trend (Fig. 5(b)). These findings are consistent with the conclusions of a previous study (Zhang et al., 2018), indicating a higher anodic potential at lower electrolyte temperatures. During the potential sweeping of the cathode, the current density peaked at around −1.48 V (MSE; see Fig. 5(c)), corresponding to the deposition of Zn (Wu et al., 2014). The polarization curves exhibited a negative shift as the electrolyte temperature decreased, resulting in the more negative potentials of Zn deposition and HER at 50 mA/cm^2. For HER, the corresponding overpotentials were estimated to increase by 102 and 70 mV at 313 and 328 K, respectively, compared to the values observed at 298 K. The higher potentials necessarily would result in higher cell voltage and PC. The weakened CE_{Zn} is mainly due to the enhanced concentration polarization of Zn deposition at lower electrolyte temperatures. Specifically, lower temperature leads to a lower diffusion rate of ions (Maslova et al., 2020) and the possible existence of a quiet Zn^{2+} concentration zone near the cathode. Thus, the Zn deposition was less selective than HER.

3.2.2 H_2SO_4 concentration

The slight influence of H_2SO_4 concentration on GF_{PM} was observed as a combined effect of surface tension and bubble characteristics. As H_2SO_4 concentration decreased, the surface tension decreased (Fig. S2(b)), contributing to fewer and smaller microbubbles and, therefore, a decreased GF_{PM}. On the other hand, a decrease in H_2SO_4 concentration slightly reduced gas generation and, thus, the size of microbubbles. Specifically, as the H_2SO_4 concentration decreased from 160 to 110 g/L, CE_{OER} and R_{O_2} were affected with increases of 0.94% and 2.45 mL/h, respectively (see Fig. 4), showing OER was slightly enhanced. However, the decrease of CE_{HER} (1.17%, Fig. 4(b)) and the decrease of R_{H2} (6.08 mL/h, Fig. 4(e)) demonstrate that lower H_2SO_4 concentration inhibited HER and therefore reduced the quantity of H_2 generated. As a result, the total gas evolution rate slightly decreased by 3.63 mL/h (1.22% of the total gas evolution rate at

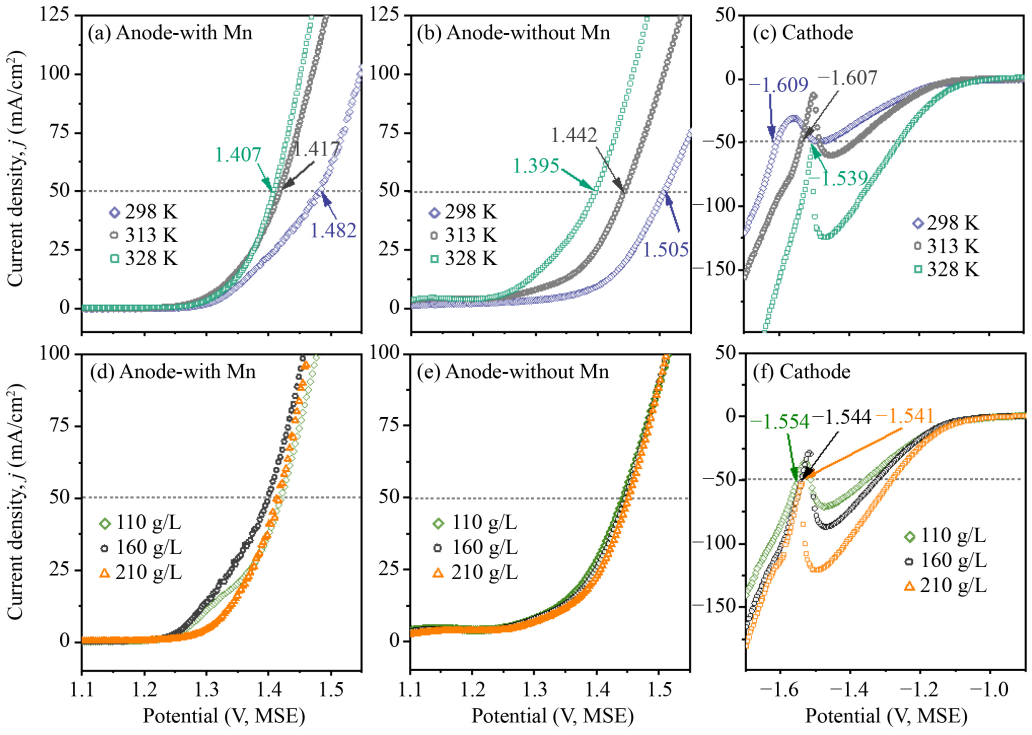

Fig. 5 Polarization curves under different operational parameters: (a–c) electrolyte temperatures; (d–f) H_2SO_4 concentrations.

160 g/L). Thus, fewer and smaller microbubbles were observed (Figs. 3(b), 3(d), and 3(e)). In addition, the more minor variations of gas evolution rate and bubble characteristics caused by H_2SO_4 concentration than that caused by electrolyte temperature accounted for the insignificant model item for predicted GF_{PM} and EF_{PM} in Section 3.1.

Variations in polarization curves and dynamic potentials at both anode and cathode at different H_2SO_4 concentrations in Figs. 5(d)–5(f). Lower H_2SO_4 concentrations resulted in larger potentials of electrode reactions, especially the cathodic reactions, compared with conventional 160 g/L. The potential to catalyze the HER is primarily controlled by the Nernstian potential for the HER, the ohmic potential drop, and the reaction overpotential (Zeng and Li, 2015). The more negative potential of HER can be mainly attributed to the lower H_2SO_4 concentration, which reduced the HER overpotential by 0.01 V and the Nernstian potential for the HER by 0.003V. This is based on the premise of no concentration gradient existing on the cathodic electrode, along with the electrolyte conductivity remaining constant (Kargl-Simard et al., 2003). Additionally, the lower H_2SO_4 concentration also noticeably made the potential of Zn deposition at 50 mA/cm^2 more negative, illustrated in Fig. 5(f). Given that the Zn^{2+} concentration and electrolyte temperature remained unchanged, the Nernstian potential remained constant. The higher overpotential of Zn deposition (calculated to be 0.03 V, excluding the influence of Zn^{2+} concentration polarization) and ohmic potential drop both contributed to an increase in the potential of Zn deposition. The results verified the higher PC at lower H_2SO_4 concentrations.

3.2.3 Current density

The mechanism of GF_{PM} reduction caused by lowering current efficiency is the synchronously reduced R_{O_2} and R_{H_2} that causes fewer and smaller microbubbles. Lower current density means reduced power supply and decreased number of electrons participating in the reaction; thus, R_{O_2} and R_{H_2} should proportionally decrease by 37.5%. R_{O_2} and R_{H_2} were lower than the theoretical value because lower current density also promoted CE_{OER} and CE_{HER} by 1.39% and 1.48% (Fig. 4(c)). Whereas the increased CE_{OER} and CE_{HER} are too little to balance the reduction due to decreased power supply. Consequently, the total gas quantity is still reduced, leading to smaller and fewer microbubbles and further GF_{PM}. The measured number and size of bubbles in Figs. 3(c)–3(e), in agreement with a previous study (He et al., 2022), verified the mechanism. The influence of surface tension on particulate matter generation resulting from bubble bursting was significant (Ghabache and Seon, 2016; Deike et al., 2022). The current density also possibly influences the surface tension, subsequently affecting particulate matter generation. However, based on the discussion about electrolyte temperature and H_2SO_4 concentration, this effect is possibly less significant in comparison to the role of electrochemical reactions. Still,

the electrolyte's surface tension could not be quantified for different current densities due to the limitation of the testing technologies.

The larger CE_{Zn} at a lower current density is related to the unaffected Zn^{2+} diffusion. Zn deposition kinetics play a significant role around 100 A/m^2 (Cai et al., 2022). However, at higher current densities (e.g., 600–1000 A/m^2), Zn^{2+} to the electrode would be exhausted quickly, resulting in a diffusion-controlled case (Cai et al., 2022), inducing a lower Zn deposition rate and thus lower CE_{Zn}. The difference of Zn^{2+} near the cathode also affects Zn deposition overpotential. Further, the overpotential of Zn deposition should be reduced because of relatively more Zn^{2+} near the cathode region at a lower current density. Lower overpotential and higher CE_{Zn} contributed to lower PC at lower current density.

4 Conclusions

Zinc electrolysis laboratory experiments were conducted to investigate methods of reducing the production of hazardous PM by controlling three operating parameters. Results show that controlling operating parameters is feasible for decreasing PM generation flux and PM emission factor. Of the three methods identified, lowering the electrolyte temperature is the most effective (89.0% reduction rate of GF_{PM}), followed by decreasing current density and decreasing H_2SO_4 concentration. However, these methods are always accompanied by higher PC or lower current efficiency of Zn deposition. The optimal combination of these three operating parameters was found by RSM methodology, which can simultaneously reduce PM generation and emission and maintain or promote Zn production and power conservation. Finally, the general reduction mechanism was inferred: reductions in electrolyte temperature, H_2SO_4 concentration, and current density inhibited the gas evolution reactions (OER and HER individually or together) to decrease the total amount of gas produced, thus reducing the number and size of microbubbles and decreasing GF_{PM}. In particular, lowering the electrolyte temperature inhibits OER and gas compression; decreasing the H_2SO_4 concentration inhibits HER and decreases surface tension. Reducing current density inhibits both OER and HER by decreasing the reaction current. Future research should concentrate on the industrial application of optimization operating parameters to minimize PM and promote Zn production. Further, developing new approaches to controlling gas generation and microbubble characteristics is also significant for PM reduction in the electrolysis process. This will ensure cleaner industrial electrolysis processes and create more sustainable industrial zinc electrolysis.

Acknowledgements This research was financially supported by the National Natural Science Foundation of China (No. 22106081), the Natural Science of Foundation of Shandong Province, China (No. ZR202103040646), the special fund of State Key Joint Laboratory of Environment Simulation and Pollution Control (China) (No. 20K09ESPCT), the Major Basic Research Projects of Natural Science Foundation of Shandong Province (China) (No. ZR2020KE025), the Fundamental Research Funds for the Central Universities (China) (No. 22120220166).

Conflict of Interest The authors Fuyuan Xu and Ning Duan are Editorial Board Members of *Frontiers of Environmental Science & Engineering*. The authors declare that the research was conducted in the absence of any commercial or financial relationships that could be construed as a potential conflict of interest.

Electronic Supplementary Material Supplementary material is available in the online version of this article at https://doi.org/10.1007/s11783-024-1762-0 and is accessible for authorized users.

References

Al Shakarji R, He Y, Gregory S (2011a). The sizing of oxygen bubbles in copper electrowinning. Hydrometallurgy, 109(1): 168–174

Al Shakarji R, He Y, Gregory S (2011b). Statistical analysis of the effect of operating parameters on acid mist generation in copper electrowinning. Hydrometallurgy, 106(1–2): 113–118

Al Shakarji R, He Y, Gregory S (2013). Performance evaluation of acid mist reduction techniques in copper electrowinning. Hydrometallurgy, 131–132: 76–80

Berny A, Popinet S, Seon T, Deike L (2021). Statistics of jet drop production. Geophysical Research Letters, 48(10): e2021GL092919

Bouakaz A, Versluis M, De Jong N (2005). High-speed optical observations of contrast agent destruction. Ultrasound in Medicine & Biology, 31(3): 391–399

Cai Z, Wang J, Lu Z, Zhan R, Ou Y, Wang L, Dahbi M, Alami J, Lu J, Amine K, et al. (2022). Ultrafast metal electrodeposition revealed by *in situ* optical imaging and theoretical modeling towards fast-charging Zn battery chemistry. Angewandte Chemie International Edition, 61(14): e202116560

Deike L, Reichl B G, Paulot F (2022). A mechanistic sea spray generation function based on the sea state and the physics of bubble bursting. AGU Advances, 3(6): 14942

Dhak D, Mahon M, Asselin E, Alfantazi A (2011). The effects of mixtures of acid mist suppression reagents on zinc electrowinning from spent electrolyte solutions. Hydrometallurgy, 108(1–2): 1–10

Dusen J V, Smith J W (1989). Comparison of the effectiveness of bubble coalescence and foamed surfactant in controlling the acid

mist formed by electrowinning cells. American Industrial Hygiene Association Journal, 50(5): 252–256

Dwivedi K A, Huang S J, Wang C T (2022). Integration of various technology-based approaches for enhancing the performance of microbial fuel cell technology: a review. Chemosphere, 287: 132248

Ghabache E, Seon T (2016). Size of the top jet drop produced by bubble bursting. Physical Review Fluids, 1(5): 051901

He H, Yu Q, Lai C, Zhang C, Liu M, Huang B, Pu H, Pan X (2021). The treatment of black-odorous water using tower bipolar electro-flocculation including the removal of phosphorus, turbidity, sulfion, and oxygen enrichment. Frontiers of Environmental Science & Engineering, 15(2): 18

He Y, Cui Y, Shang W, Zhao Z, Tan P (2022). Insight into the bubble-induced over potential towards high-rate charging of Zn-air batteries. Chemical Engineering Journal, 448: 137782

Ji S L, Weon B M, Su J P, Je J H, Fezzaa K, Lee W K (2011). Size limits the formation of liquid jets during bubble bursting. Nature Communications, 2(1): 367

Kargl-Simard C, Huang J H, Alfantazi A M (2003). Electrical conductivity and density of $CoSO_4/H_2SO_4$ solutions in the range of modern cobalt electrowinning electrolytes. Minerals Engineering, 16(6): 529–535

Ke W R, Kuo Y M, Lin C W, Huang S H, Chen C C (2017). Characterization of aerosol emissions from single bubble bursting. Journal of Aerosol Science, 109: 1–12

Lasia A (2019). Mechanism and kinetics of the hydrogen evolution reaction. International Journal of Hydrogen Energy, 44(36): 19484–19518

Luo J, Jiao P, Duan N, Xu F, Jiang L (2018). Flow field characterization in the vicinity of vertical plane electrodes in a bench-scale zinc electrowinning cell. Hydrometallurgy, 181: 103–112

Ma Z, Duan L, Jiang J, Deng J, Xu F, Jiang L, Li J, Wang G, Huang X, Ye W, Wen Y, Zhang G, Duan N (2020a). Characteristics and threats of particulate matter from zinc electrolysis manufacturing facilities. Journal of Cleaner Production, 259: 120874

Ma Z, Jiang J, Duan L, Li Z, Deng J, Li J, Zhang R, Zhou C, Xu F, Jiang L, Duan N (2020b). Ultrasonication to reduce particulate matter generated from bursting bubbles: a case study on zinc electrolysis. Journal of Cleaner Production, 272: 122697

Maslova M V, Ivanenko V I, Yanicheva N Y, Mudruk N V (2020). Comparison of the sorption kinetics of lead(II) and zinc(II) on titanium phosphate ion-exchanger. International Journal of Molecular Sciences, 21(2): 447

Mason T J, Lorimer J P, Saleem S, Paniwnyk L (2001). Controlling emissions from electroplating by the application of ultrasound. Environmental Science & Technology, 35(16): 3375–3377

Mcginnity J J, Nicol M J (2014). Sulfuric acid mist: generation, suppression, health aspects, and analysis. Mineral Processing and Extractive Metallurgy Review, 35(3): 149–192

Mokarram M, Pourghasemi H R, Zhang H (2020). Predicting non-carcinogenic hazard quotients of heavy metals in pepper (*Capsicum annum* L.) utilizing electromagnetic waves. Frontiers of Environmental Science & Engineering, 14(6): 114

Papachgristodoulou A, Foulkes F R, Smith J W (1985). Bubble characteristics and aerosol formation in electrowinning cells. Journal of Applied Electrochemistry, 15(4): 581–590

Qu C, Li K, Xie Z, Yang S, Zhao J, Sun D, Sun Y (2022). Stacking polymer microspheres matrix: a facile, practical, and energy-saving strategy for suppression of acid mist. Environmental Technology, 44: 18, 2693–2701

Shaw L, Shaw D, Hardisty M, Britz-Mckibbin P, Verma D K (2020). Relationships between inhalable and total hexavalent chromium exposures in steel passivation, welding and electroplating operations of Ontario. International Journal of Hygiene and Environmental Health, 230: 113601

Sorour N, Zhang W, Ghali E, Houlachi G (2017). A review of organic additives in zinc electrodeposition process (performance and evaluation). Hydrometallurgy, 171: 320–332

Theerthagiri J, Madhavan J, Lee S J, Choi M Y, Ashokkumar M, Pollet B G (2020). Sonoelectrochemistry for energy and environmental applications. Ultrasonics Sonochemistry, 63: 104960

Wang X, Deane G B, Moore K A, Ryder O S, Stokes M D, Beall C M, Collins D B, Santander M V, Burrows S M, Sultana C M, Prather K A (2017). The role of jet and film drops in controlling the mixing state of submicron sea spray aerosol particles. Proceedings of the National Academy of Sciences of the United States of America, 114(27): 6978–6983

Wu X, Liu Z, Liu X (2014). The effects of additives on the electrowinning of zinc from sulphate solutions with high fluoride concentration. Hydrometallurgy, 141: 31–35

Xu K, Lu J, Tegladza I D, Xu Q, Yang Z, Lv G (2020a). Combined metal/air fuel cell and electrocoagulation process: energy generation, flocs production and pollutant removal. Chemosphere, 255: 126925

Xu X, Li D, Chen L, Liu M, Jia J J H (2020b). Improve the energy efficiency: effects of additives on longtime zinc electrowinning. Hydrometallurgy, 193: 105326

Xue T, Xu L, Wang Q (2019). Measurement of seawater surface tension coefficient based on bubble rising behavior. Measurement, 138: 332–340

Zeng M, Li Y (2015). Recent advances in heterogeneous electrocatalysts for the hydrogen evolution reaction. Journal of Materials Chemistry. A, Materials for Energy and Sustainability, 3(29): 14942–14962

Zhang C, Duan N, Jiang L, Xu F (2018). The impact mechanism of Mn^{2+} ions on oxygen evolution reaction in zinc sulfate electrolyte. Journal of Electroanalytical Chemistry (Lausanne, Switzerland), 811: 53–61